Data Science and Advanced Python Project: Reproduced Published Results

Don Enrico Esteve (P9550217B) and Elizabeth Vaisman (318775277)

Introduction

Selected article

Analysis of Functional Connectivity and Oscillatory Power Using DICS: From Raw MEG Data to Group-Level Statistics in Python (van Vliet et al., 2018)

Article summary

Based on a standard, freely available MEG dataset obtained by Wakeman and Henson (2015), the pipeline presented consists of seven (7) sections: (i) preprocessing, (ii) estimation of cross-spectral density (CSD) matrices, (iii) across-subject source transformation, (iv) estimation of oscillatory activity, (v) coherence computation, (vi) group-level statistics, and (vii) visualization of identified networks. Along with code examples, this led to the development of a new Python package *ConPy* (van Vliet et al., 2018) that well-integrates with *MNE* (Gramfort et al., 2013), a well-documented package for M/EEG data analysis in Python. With this pipeline, they compared the changes in oscillatory activity and functional connectivity between processing normal and scrambled faces, based on dynamic imaging of coherent sources (DICS), at 6 frequency bands.

Rationale for selection and objectives

This protocol article, which highlights MEG for neuroscience and promotes the use of free academic software for MEG analysis, reinforces both theoretical knowledge and practical skills obtained from the MEG-BIU laboratory. Reproducing an article that delves into induced responses in the time-frequency domain was interesting as capturing brain oscillatory activity and functional connectivity not only reflects important cognitive processes but may also have predictive value for subsequent behavior (Hermann et al., 2013).

While this project aims to reproduce published results, after all, the article aims to outline the full implementation of oscillatory activity and functional connectivity analyses. As such, we aim to translate their proposed pipeline to a MEG dataset obtained from the MEG-BIU lab (called “food dataset” in subsequent sections). Effectively, this explores the food dataset at the time- and time-frequency domains. The dataset contains preprocessed MEG recordings from 42 subjects who underwent a visual repetition experiment. It was divided into 3 blocks of differing lag durations (short, medium, and long), during which the participants observed 3 image categories: high-caloric food, positive non-food (e.g., flowers, puppies, and babies), and neutral objects. In an oddball task, each image was shown twice in a block.

Methodology

Pipeline replication

The code repository for this article contains twelve (12) Python scripts for reproducing the pipeline, from fetching the dataset to performing across-subject connectivity statistics. These scripts were used with minor modifications (e.g., replacing deprecated methods, refraining from using dependencies incompatible with the latest module versions, etc.). The total run time for replication was ~one week, as the processing of anatomical MRI using the *recon_all* method of FreeSurfer (Fischl, 2012) presented a major computational bottleneck. For this step, the authors

reported a run time of ~one day per subject (n=17). During replication on a 2.3 GHz 8-Core Intel Core i9 Macbook Pro with 16 GB of memory, the run time was reduced to ~6 hours per subject. This also included extracting a 3-layer boundary element method (BEM) model from flash MRI.

Band-pass filtering was performed from 1-40 Hz in preprocessing the raw MEG signals. Also, artifacts (e.g., heartbeats, eye blinks) were removed by Independent Component Analysis (ICA) decomposition in which components explaining 99.9% of the cumulative variance were retained. Trials were decimated by taking only every 5th sample (~200 Hz sampling rate), then epoched from -0.2 to 2.9 s from stimulus onset. Relative to baseline (-0.2 to 0 s), cross-spectral density (CSD) was estimated using Morlet wavelets during the time of interest (0 to 0.4 s) for each frequency band (see code). A source space was created on the template *fsaverage* brain from FreeSurfer, then morphed to that of each subject. Using the BEM model and source space (Fig. 1a), a forward model was defined for each subject (Fig. 1b).

For power mapping, a regularized (5%) DICS beamformer was computed using the CSD matrices and forward models, for each condition, frequency band, and subject. Relative to the baseline, the difference in power between the two experimental conditions was computed. The coherence-based all-to-all connectivity for the low gamma band (31-39 Hz) was computed for each condition and subject. Cortical power maps and connectivity estimates for the normal and scrambled conditions, and their contrast, were averaged across subjects. Finally, the averaged connectivity estimates were tested for significant clusters, pruned, and parcellated.

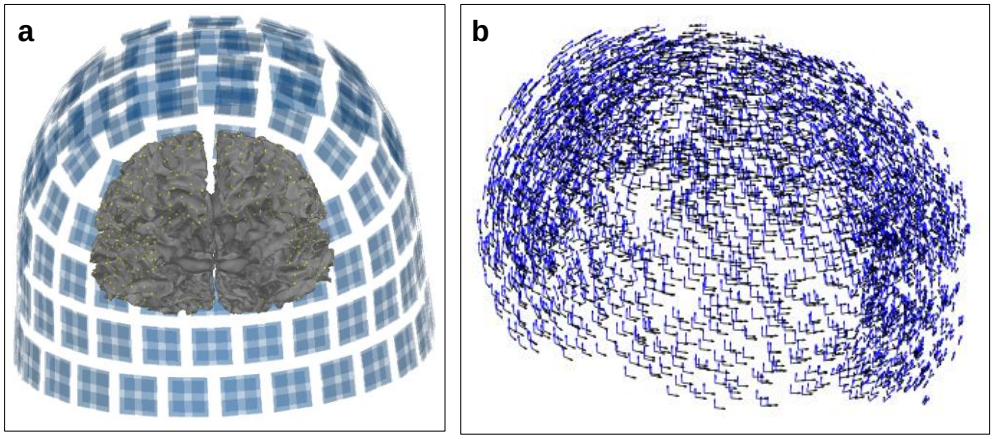

Fig. 1. (a) 3D alignment of the sensors (blue), brain layer of the BEM model or head model (gray), and the source space or source model (yellow) of Subject 1. Points of the source space further than 7 cm from the closest MEG sensor were discarded. **(b)** The forward model or lead field, defining two tangential dipoles at each source point, of Subject 1. These are exact replicates of those from van Vliet et al. (2018).

Pipeline implementation

The MEG recordings have already been preprocessed using *FieldTrip* (Oostenveld et al., 2010) in Matlab. Signals were band-pass filtered from 1-30 Hz, and decomposed using ICA. Trials were epoched from -0.3 to 0.8 s relative to the stimulus onset. For each subject, the preprocessed file (.mat) was converted (.fif), and read as instances of class Epochs in *MNE*. While both sensor- and source-level analyses were intended, pipeline implementation was successful only for the former due to: (i) lack of subject-specific anatomical MRI, (ii) difficulties in template MRI estimation

using *MNE*, and (iii) non-convertible head and source models from *FieldTrip* to *MNE*. Instead, sensor-level time-frequency analyses were performed, yielding several plots for time-frequency representation (TFR). Pipeline implementation was performed on a single subject (Subject 003).

Results and discussion

Pipeline replication

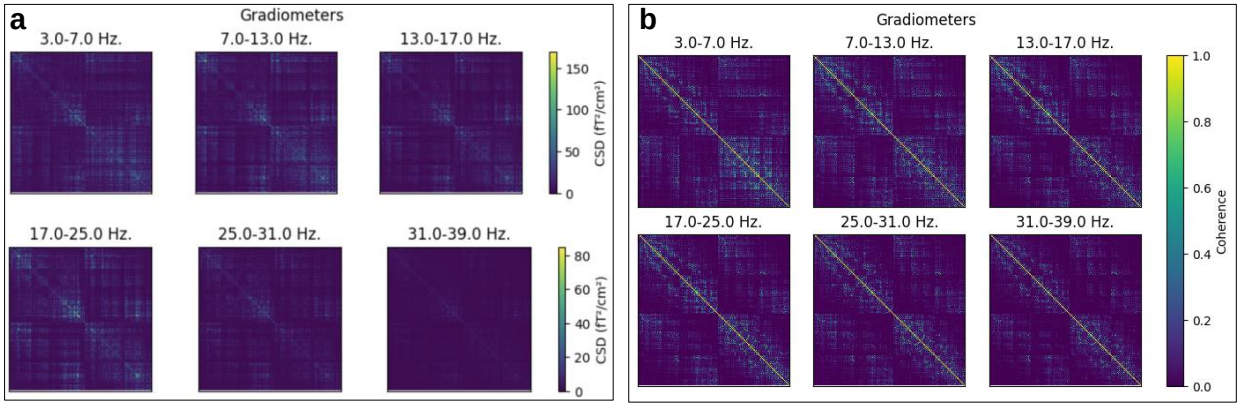

Fig. 2. (a) CSD and **(b)** coherence matrix for each frequency band (n=6) where a normal face stimulus was presented to Subject 1. Each row and column represents a gradiometer (n=204). The first 3 frequency bands differ in scale from the latter 3 bands.

Both the CSD (Fig. 2a) and coherence (Fig. 2b) matrices show that connection between and across gradiometers decreases with increasing frequency bands, with most high-valued pixels present in the theta band (3-7 Hz) and otherwise in the low gamma band (31-39 Hz). Notably, gradiometers with indices around the middle (~102) show higher CSD and coherence than all other pairs. These are also apparent for the scrambled face stimulus and other subjects.

More importantly, these trends and patterns coincide with the CSD matrices of van Vliet et al. (2018). The difference is found only in the CSD values, with the replicated results having slightly lower CSD values for the first three bands, but higher CSD values for the latter three. The addition of coherence matrices is an improvement over the original article.

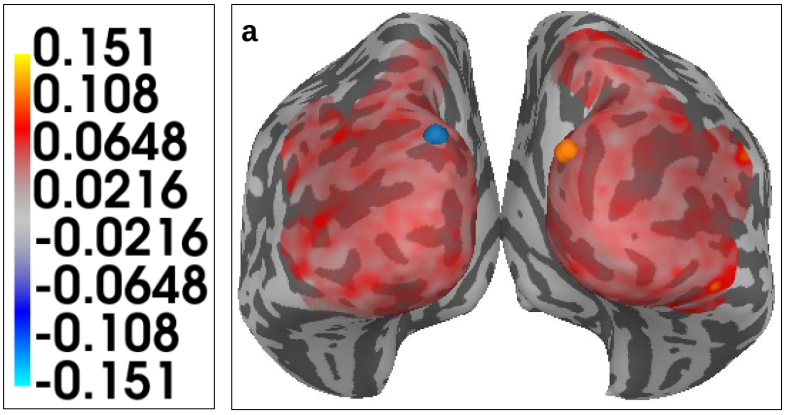

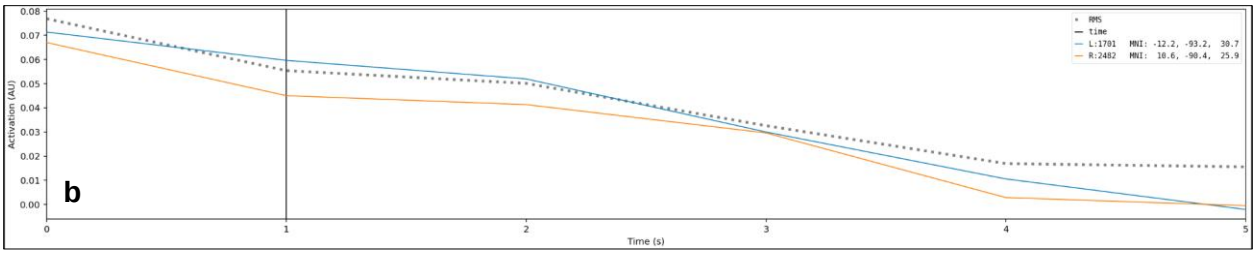

Fig. 3. (a) Grand average power map of the contrasting condition (face – scrambled / baseline), for the alpha band (7-13 Hz), taken at 1 s. A caudal view of each hemisphere is shown. Warmer colors indicate sources with more activity for faces than scrambled images. **(b)** Activation plot for each hemisphere over time.

Across subjects, there is greater bilateral activity in visual areas when normal faces are presented (Fig. 3a). This coincides with the well-established finding that normal faces are better recognized than scrambled faces across primates and paradigms (George et al., 1996; Taubert et al., 2012). Over time, the left hemisphere was more active (Fig. 3b), contradicting the known lateralization of face recognition on the right hemisphere. However, some studies note a left hemisphere advantage when the comparisons are based on discrete facial features (Rhodes, 1985). Regardless, the difference in activation units between hemispheres is relatively minimal.

Relative to van Vliet et al. (2018), the replicated grand average power for the alpha band of contrast condition has higher activity and is more restricted in cortical distribution. While this replicated activity is present only on the occipital areas, that in the article has activity on other lobes that may be not related to early visual processing. Also, the authors failed to report the corresponding activation plot. These are considered improvements in cortical power mapping.

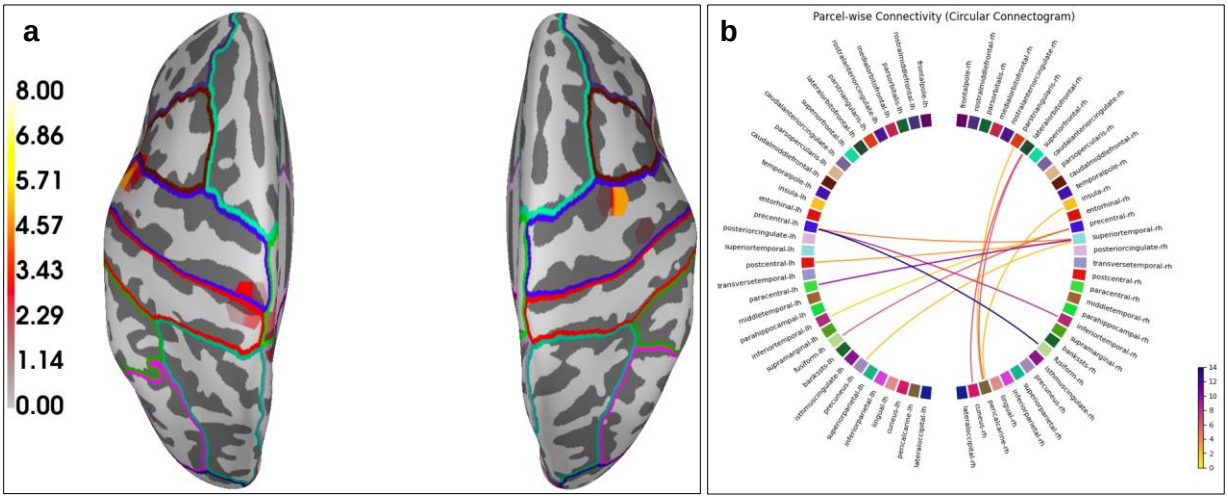

Fig. 4. (a) Degree map showing, for each source point, the surviving connections after statistical pruning. A dorsal view of each hemisphere is shown. **(b)** Circular connectogram, arranged by hemisphere, showing the number of connections between each parcel. These plots, averaged across subjects, show the connectivity for the low gamma band of the contrast condition.

Both connectivity plots (Fig. 4) reveal that induced brain activity remains well-connected even at higher frequencies. From a dorsal view, there are ≥2 bundles of connections (Fig. 4a).

The highest number of connections (n=14) are present between the left precentral and right fusiform gyri (Fig. 4b). This implies that respective oscillatory activity in these parcels is more synchronous or coherent than all other parcel pairs. Facial processing has been documented to occur in the right fusiform gyrus, leading to the establishment of functional areas such as the right fusiform face area (Watanabe et al., 1999; Rossion, 2003). Overall, there seem to be more inter-hemispheric connections than intra-hemispheric connections, with the latter apparent only on the right. This suggests that connectivity estimates, rather than cortical power, may better represent the right hemisphere advantage for face recognition.

The circular connectogram of van Vliet et al. (2018) does not reveal the connections to and from the right fusiform gyrus, and this may be due to their extensive cluster permutation test (n_permutations = 1000) for finding significant bundles. Meanwhile, our approach of finding the raw connections by markedly downscaling the permutation test (n_permutations = 1) revealed the importance of the right fusiform gyrus in this particular experimental paradigm. This may be the largest improvement over the original article.

Pipeline implementation

The succeeding plots (Figs. 5-9) reflect sensor-level results. Among these, only Fig. 5 show time-domain results and the remaining are of time-frequency domain. Various combinations of conditions were shown and contrasted, whenever possible, to demonstrate the larger extent of the food dataset. In the time-frequency domain, various frequency bands between 1-30 Hz were analyzed as van Vliet et al. (2018) did: theta (3-7 Hz), alpha (7-13 Hz), low beta (13-17 Hz), high beta 1 (17-25 Hz), and high beta 2 (25-31 Hz). For calculating TFRs, various methods were used, such as Morlet wavelet and multitaper, for exploratory purposes.

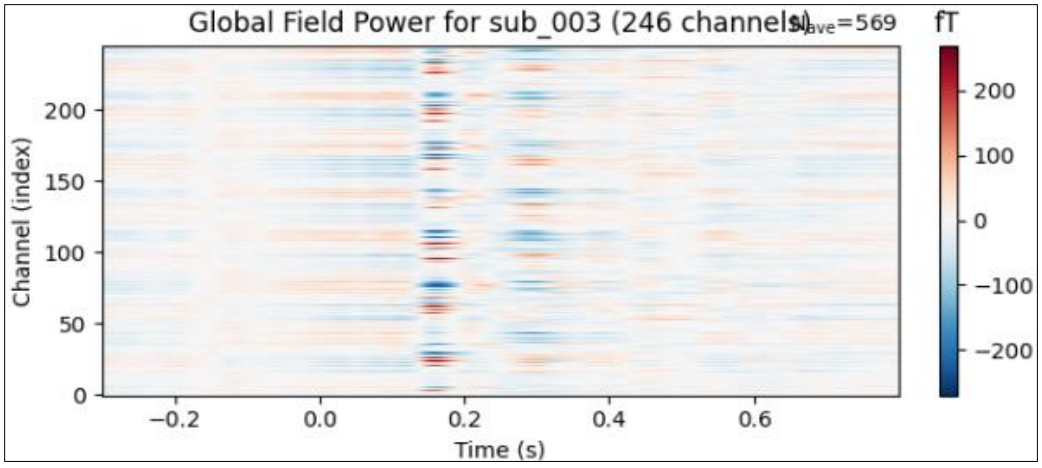

Fig. 5. Global field power (GFP) showing the sensor-wise (n = 246 magnetometers) temporal dynamics of ERF across conditions (n = 18), for Subject 003. Regardless of value, darker colors reflect higher ERF magnitudes (~1e-15 Tesla, fT). Across sensors, the GFP peaks during two time windows: close to 0.2 s (M190) and around 0.3 s (M300).

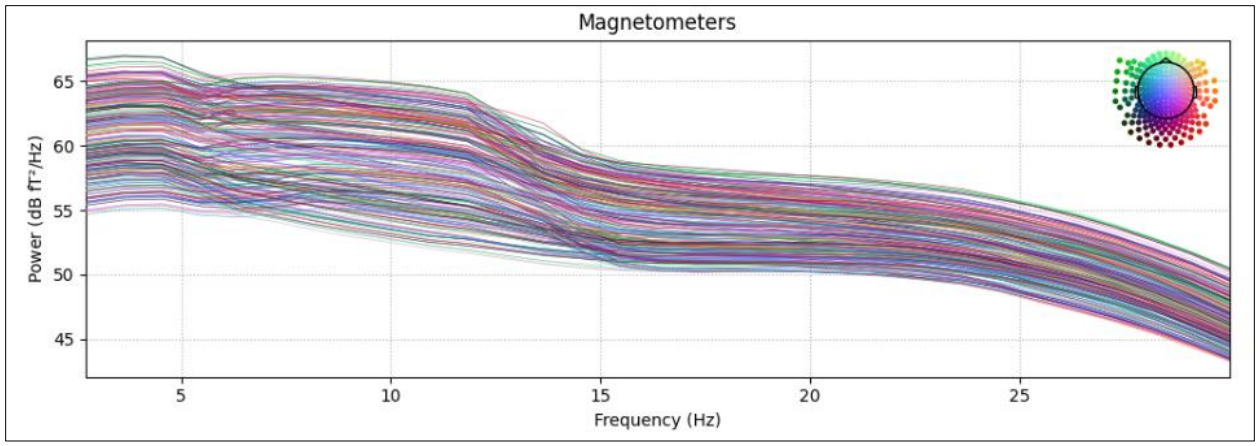

Fig. 6. Power spectral density (PSD) across frequencies (2-30 Hz), time (-0.3-0.8 s), and sensors for Subject 003. The estimated power is measured in decibels (dB). Spectrum lines are colored based on sensor location (top right). The usual trend of decreasing spectral power with increasing frequency is apparent. At relatively lower bands (i.e., theta to alpha) and higher bands (i.e., beta), the PSD respectively exhibits gradual and sharp decreases.

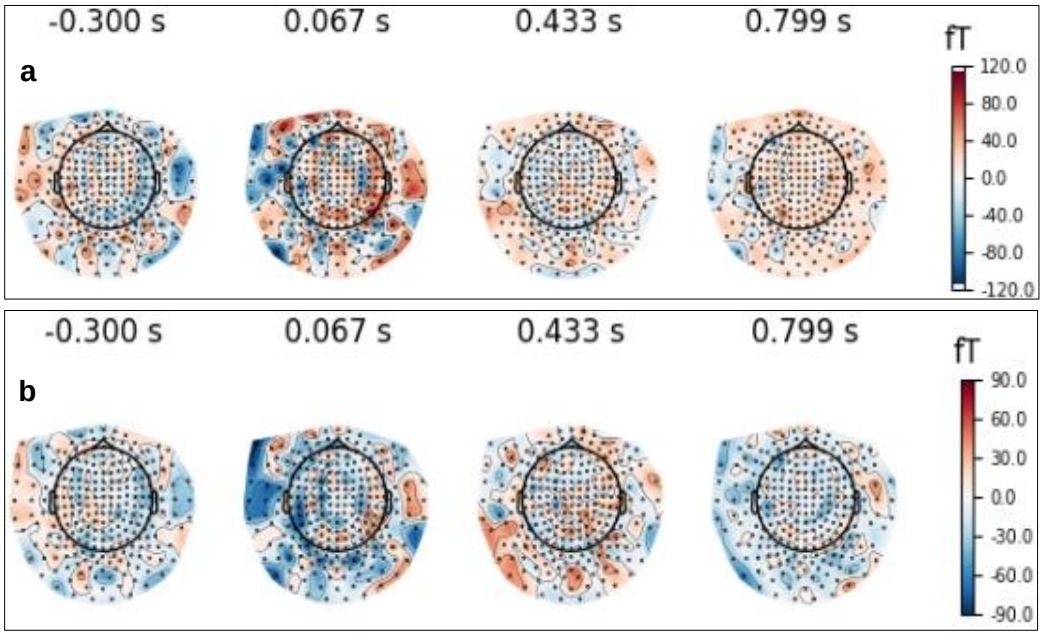

Fig. 7. Topographic maps, based on local extrapolation, across frequency (1-30 Hz) for the **(a)** 1st presentation and **(b)** 2nd presentation of food images, for Subject 003. Relative to baseline (leftmost maps), there is higher activation across the post-stimulus window (succeeding maps). Among these, peak activation occurs shortly after stimulus onset (0.067 s), present in the left anterior, right temporal and posterior sensors.

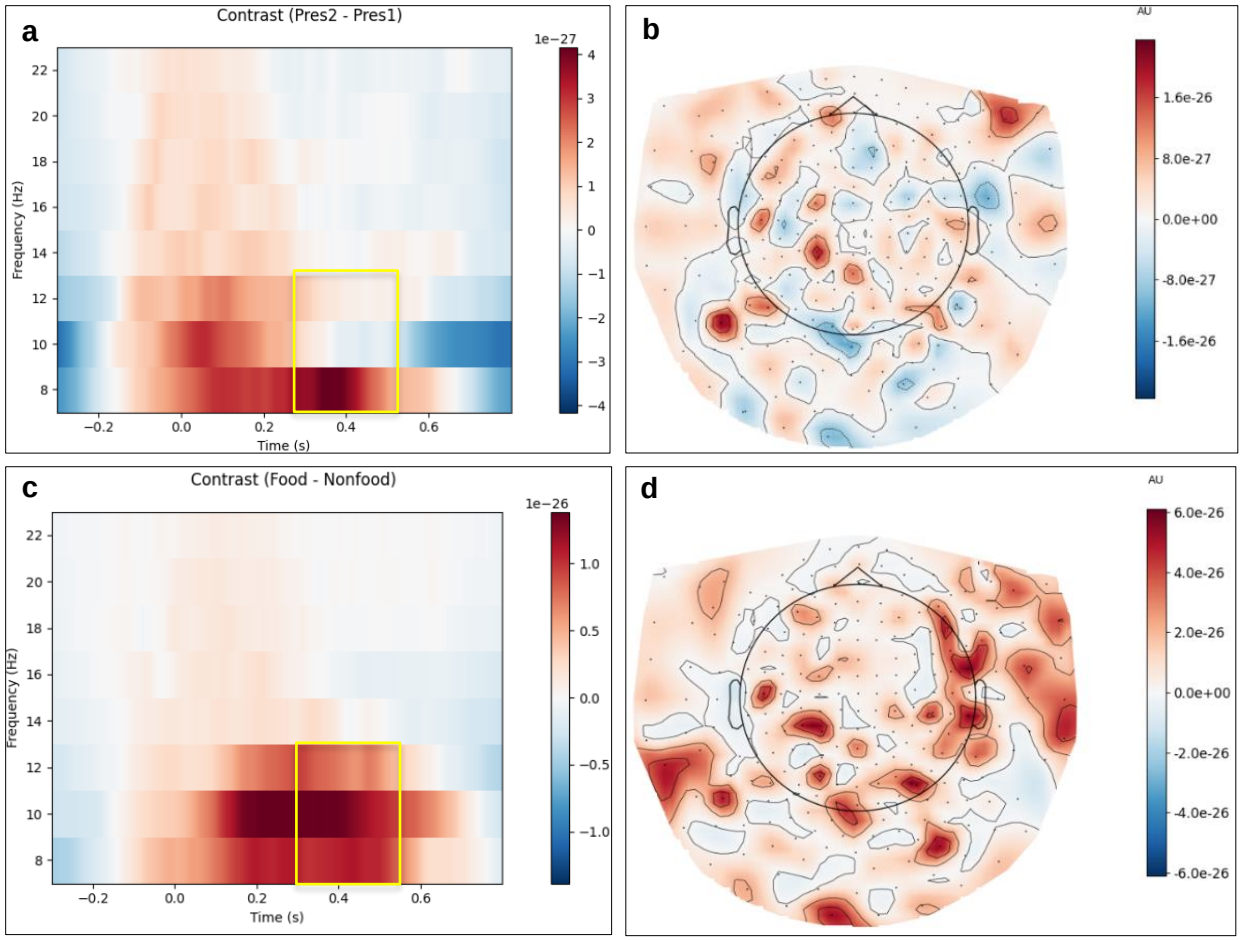

Fig. 8. Time-frequency representation (TFR) of the difference in response between: **(a)** 1st and 2nd presentation, regardless of image category and lag duration; **(c)** food and non-food (positive and neutral images), regardless of presentation and lag duration. TFRs were calculated using the multitaper method and averaged across sensors. The **(b and d)** topographic maps roughly represents the boxed regions (yellow) in their respective TFRs. All plots are for Subject 003.

Various contrasts between experimental conditions differ in temporal-spectral (Fig. 8a and 8c) and spatial (Fig. 8b and 8d) patterns. For both contrasts, the respective difference in activity temporally peaks later (0.2-0.4 s) relative to stimulus onset and spectrally peaks within the alpha band. This coincides with the observations of van Vliet et al. (2018), although at the source level, that activity tends to be dominated by alpha and beta activity. The appreciable difference in activity appears broadband between presentations than that between image categories (Fig. 8c). The magnitude, however, is greater for the latter contrast. Also, the sensors located in areas identified in Fig. 7 are where the peak TFR differences localize. This may indicate activation of the occipital and temporal cortices, respectively corresponding to visual response and visual memory.

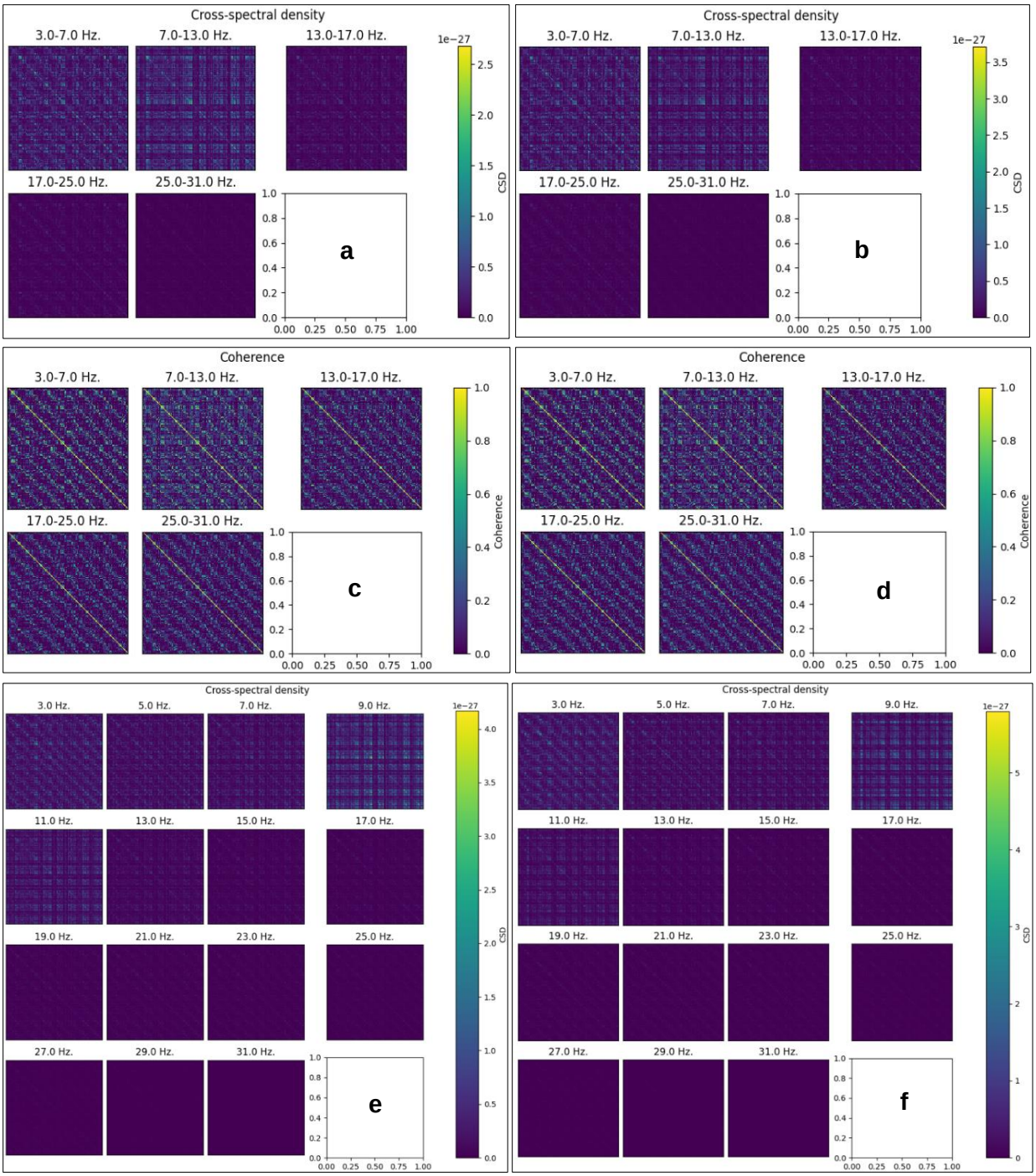

Fig. 9. Mean CSD and coherence matrices **(a-d)** averaged over the defined frequency bands, analogous to those of van Vliet et al. (2018), for the 1st presentation of food images for Subject 003. For a more comprehensive view, CSD matrices **(e-f)** per frequency are presented as well. The **(a, c, e)** baseline (-0.3-0 s) matrices serve as reference for their respective **(b, d, f)** post-stimulus (0-0.8 s) matrices. CSD matrices, computed using the Morlet wavelet method, are pre-requisite for the intended source-level analysis in the time-frequency domain.

The CSD matrices show, for a given frequency or frequency band, the correlation between the TFR of each sensor pair. Across sensor pairs, the peak magnitude of CSD values is higher during the post-stimulus window (Fig. 9b, 9d, 9f) relative to those during the baseline (Fig. 9a, 9c, 9f). The trend of decreasing CSD values with increasing frequency is apparent (Fig. 9a-9b), which was also found in the original (van Vliet et al., 2018) and replicated (Fig. 2a) CSD matrices. The grid-like pattern in magnetometer connections (Fig. 9a-9b), as expected, differs from the patterns in gradiometer connections of the reference CSD matrices. In terms of coherence, there are no appreciable difference between the time windows (Fig. 9c-9d).

The per frequency CSD matrices (Fig. 9e-9f) support Fig. 9a-9b, showing that most sensor connections are spectrally localized at theta and alpha frequencies. Among these, CSD values seemingly peak at 9 Hz. The diagonal connections weaken during the post-stimulus window (Fig. 9f), relative to baseline (Fig. 9e), yet the magnitude increases across sensor pairs.

Conclusion

The pipeline replication is successful, however, it did not yield the exact results as the pipeline was performed on one more subject (n=17). The authors failed to report which three subjects (only two bad subjects were reported) they excluded in their analyses. Still, replicating this project fulfilled the shared primary objective of comparing changes in oscillatory activity and functional connectivity between processing normal and scrambled faces. Despite only covering sensor-level analyses, the pipeline implementation yielded intuition on the temporal, spectral, and spatial characteristics of the MEG signals in the food dataset. This project serves as a foundation for further analyzing the food dataset in the time-frequency domain. Overall, this project prompted utilizing neuroimaging software (e.g., FreeSurfer) and programming cross-platform, from *FieldTrip* in Matlab to *MNE* in Python, ultimately cultivating data science techniques for neuroscience.

References

Fischl, B. (2012). FreeSurfer. NeuroImage, 62(2), 774–781. https://doi.org/10.1016/j.neuroimage.2012.01.021

George, N., Evans, J., Fiori, N., Davidoff, J., & Renault, B. (1996). Brain events related to normal and moderately scrambled faces. *Cognitive Brain Research, 4*(2), 65–76. https://doi.org/10.1016/0926-6410(95)00045-3

Gramfort, A., Luessi, M., Larson, E., Engemann, D. A., Strohmeier, D., Brodbeck, C., Goj, R., Jas, M., Brooks, T., Parkkonen, L., & Hämäläinen, M. (2013). MEG and EEG data analysis with MNE-Python. *Frontiers in Neuroscience, 7*, Article 267. https://doi.org/10.3389/fnins.2013.00267

Herrmann, C. S., Rach, S., Johannes Vosskuhl, & Strüber, D. (2013). Time–Frequency Analysis of Event-Related Potentials: A Brief Tutorial. *Brain Topography, 27*(4), 438–450. https://doi.org/10.1007/s10548-013-0327-5

Oostenveld, R., Fries, P., Maris, E., & Jan-Mathijs Schoffelen. (2010). FieldTrip: Open Source Software for Advanced Analysis of MEG, EEG, and Invasive Electrophysiological Data. *Computational Intelligence and Neuroscience*, 1–9. https://doi.org/10.1155/2011/156869

Rhodes, G. (1985). Lateralized processes in face recognition. *British Journal of Psychology, 76*(2), 249–271. https://doi.org/10.1111/j.2044-8295.1985.tb01949.x

Rossion, B. (2003). A network of occipito-temporal face-sensitive areas besides the right middle fusiform gyrus is necessary for normal face processing. *Brain, 126*(11), 2381–2395. https://doi.org/10.1093/brain/awg241

Taubert, J., Aagten-Murphy, D., & Parr, L. A. (2012). A Comparative Study of Face Processing Using Scrambled Faces. *Perception, 41*(4), 460–473. https://doi.org/10.1068/p7151

van Vliet, M., Liljeström, M., Aro, S., Riitta Salmelin, & Kujala, J. (2018). Analysis of Functional Connectivity and Oscillatory Power Using DICS: From Raw MEG Data to Group-Level Statistics in Python. *Frontiers in Neuroscience, 12*. https://doi.org/10.3389/fnins.2018.00586

Wakeman, D. G., & Henson, R. N. (2015). A multi-subject, multi-modal human neuroimaging dataset. *Scientific Data, 2*(1). https://doi.org/10.1038/sdata.2015.1

Watanabe, S., Kakigi, R., Koyama, S., & Kirino, E. (1999). Human face perception traced by magneto- and electro-encephalography. *Cognitive Brain Research, 8*(2), 125–142. https://doi.org/10.1016/s0926-6410(99)00013-0